Corrosion Science 227 (2024) 111669

Contents lists available at ScienceDirect

Corrosion Science

journal homepage: www.elsevier.com/locate/corsci

In-situ measurement of electrochemical activity related to filiform corrosion in organic coated steel by scanning vibrating electrode technique and scanning micropotentiometry

Andrea Cristoforetti [a,*], Javier Izquierdo [b], Ricardo M. Souto [b], Flavio Deflorian [a], Michele Fedel [a], Stefano Rossi [a]

[a] Department of Industrial Engineering, University of Trento, via Sommarive n. 9, 38123 Trento, Italy
[b] Institute of Material Science and Nanotechnology, University of La Laguna, P.O. Box 456, Tenerife, Canary Islands, E-38207 La Laguna, Spain

ARTICLE INFO

Keywords:
A: Organic coatings
A: Steel
B: Scanning vibrating electrode technique
B: Scanning electrochemical microscopy
B: Potentiometry
C: Anodic dissolution
C: Atmospheric corrosion
C: Paint coatings

ABSTRACT

A new approach to studying the mechanism of filiform corrosion in organic coated steel based on the scanning vibrating electrode technique (SVET) and micropotentiometry (potentiometric SECM) is presented. The electrochemical activity of the process under the coating is evaluated by mapping the ionic current densities emanating from some artificial defects made in specific locations of the filament identifiable thanks to the transparency of the coating. In addition, antimony tips are employed to investigate the pH changes associated to the different corrosion reactions at the metal-paint interface. Local pH levels associated to anodic and cathodic regions are determined along the filament.

1. Introduction

Knowledge of the electrochemical reactions on which the corrosion mechanism is based is essential for the design of any prevention and mitigation strategy. Despite several decades of research in this field, the aspects of the different phenomena involved are still not fully known. Some models in the literature are based on reasonable assumptions but still lack experimental evidence. Several limitations arise in the field of organic coated metals because the covering insulating layer makes it difficult to gain information about the environment at the metal-paint interface.

Filiform corrosion (FFC) of organic coated carbon steel is an example of a mechanism that is still under investigation, as it presents several unresolved questions related to causes, mechanisms, and reactions [1–3]. The FFC is recognized as a special case of an oxygen-concentration cell characterized by a peculiar thread-like morphology. Under the paint, it is possible to distinguish the leading head from the growing tail thanks to the marked color gradient, respectively green and brown [2,3]. FFC occurs more frequently than expected, requiring only a relative humidity between 65%– 95% and mild chloride contamination to be triggered [3,4]. However, we believe it is often confused with cathodic delamination [5] because it is not recognized due to the presence of pigments in the paint, which can hide its peculiar morphology. Despite it being commonly defined as an aesthetical type of degradation, the actual contribution to the coating system failure is severe since the filament propagation causes a dramatic paint delamination. Moreover, once the detached coating is no longer able to protect the metal substrate other mechanisms of corrosion could be easily involved affecting the structure integrity [6].

Various mechanistic models are reported in the literature to describe FFC in organic-coated carbon steel, sometimes contradicting each other [3,7–9]. In a previous article [2], we tried to give an overview of the current understanding, and, together with some new experimental findings, we presented an updated model of FFC comprehensive of all the information found in the literature. However, it was based on certain assumptions regarding (i) the contribution and role of the tail in filament propagation, and (ii) the composition and chemical properties of the environment formed at the metal-paint interface. One of the debated aspects of FFC is that the location of the anodic and cathodic sites is not yet clearly identified. In fact, several studies reported the occurrence of cathodic delamination in the leading part of the filaments [7,10], a feature that is not in accordance with the common belief of an anodic

* Corresponding author.
E-mail address: andrea.cristoforetti@unitn.it (A. Cristoforetti).

https://doi.org/10.1016/j.corsci.2023.111669
Received 4 August 2023; Received in revised form 13 October 2023; Accepted 11 November 2023
Available online 16 November 2023
0010-938X/© 2023 The Author(s). Published by Elsevier Ltd. This is an open access article under the CC BY license (http://creativecommons.org/licenses/by/4.0/).

undermining phenomenon [2–4,8,11]. Others have hypothesized that the location of the cathodic site is the back part of the green head rather than the growing tail [12]. In addition, several publications dealing with FFC have made assumptions or measured approximate values of the pH developed in the growing filament [13–15]. To the best of our knowledge, the only experimental evidence reported in the literature is based on indicator papers placed at a metal-paint interface after the removal of the coating. In this context, the need for more robust pH measurements is also evident because of the precious hints about the mechanism that the pH distribution could give. Knowing the pH value developed at a specific corrosion spot will allow us to infer the ongoing electrochemical reactions. Therefore, it is worth making more scientific efforts in this direction, exploring the applicability of new techniques and approaches to this aged but unsolved issue that combines spatial and chemical information in operando.

Electrochemical Impedance Spectroscopy (EIS) is a common tool to detect coating degradation [16–18]. It has proven to be suitable in the early stages of corrosion to detect the presence of defects in the paint [19,20] or water uptake [21,22]. However, it gives an average response over all exposed areas, and although it is possible to distinguish the various contributions by modeling an electrical equivalent circuit [23], the spatial distribution of those contributions over the surface cannot be resolved [24]. For this reason, EIS is not particularly useful for investigating the mechanism of localized corrosion. In this context, several localized techniques have been introduced to overcome the limitations of conventional electrochemical measurements [14]. Regarding paint delamination, Scanning Kelvin Probe (SKP) was employed to detect the propagation of cathodic delamination [25], changes in interface bonding during water uptake [26], and also for the investigation of filiform corrosion [1,10,27]. However, in the latter case, SKP has proven not always accurate in distinguishing the different active sites underneath the paint in a propagating filament, and the distribution of anodic and cathodic zones has not yet been deciphered [2,10]. In addition, only local distributions of Volta potential in the metal can be obtained using SKP, without providing any chemical information on the chemical species involved in the different sites composing the electrochemical system responsible for the onset of FFC. For this reason, it is considered that microelectrochemical techniques would be regarded as powerful techniques for the study of FFC as has occurred with other case studies on organic coated metals [28–31] when either spontaneously presenting defects or after producing artificial defects through the coating layer (namely scratches, cut edges, etc), thus producing the electrolytic environment to get in direct contact with the metal substrate. Unfortunately, FFC occurs under a non-defective coating and in the absence of a direct exposure to an external electrolytic phase of environmental origin, thus preventing scanning microelectrochemical methods to have access to the buried interface under the insulator layer that is required to the development of FFC.

Scanning Reference Electrode Technique (SRET) [32,33], Scanning Vibrating Electrode Technique (SVET) [24,34–37], Local Impedance Spectroscopy (LEIS) [38–40], Scanning Electrochemical Microscopy (SECM) [28,36,40] and scanning micropotentiometry (also known as SECM in potentiometric mode, and Scanning Ion Electrode Technique, SIET) [29,41,42] are the most widely used localized techniques in the field of corrosion. When it comes to FFC, in our opinion, SVET could be powerfully exploited since it is able to distinguish between anodic and cathodic areas [37,43]. The scanning of a vibrating probe over an immersed sample gives us the distribution of the electric potential in that area thanks to the local gradient in the electrolyte. To measure a signal, some charged species must be present, and in the case of samples that corrode, they are usually consumed or released by the metal surface. When an intact organic coating is present, even if the ionic activity under the paint is well developed, no signal can be obtained by SVET and the other localized techniques mentioned above as the organic coating acts as a physical barrier preventing the transport of the corrosion products to the aqueous electrolytic environment. For this reason, all the studies available in the corrosion field solely investigate the behavior of bare metals or defective coatings [32,43–46], with the only exception of water uptake by a non-defective organic coating using scanning electrochemical microscopy [47–49], which actually was purely a topographical microscopic observation without exploiting the chemical resolution of the technique.

Since FFC morphology develops right underneath the organic layer and the species needed to sustain the reactions are provided by the path created from a defect through the filament tail, an alternative approach has to be employed to exploit the performances of the SVET. In this study, a novel strategy based on SVET to determine the anodic and cathodic areas along a growing filament at the metal-paint interface was introduced exploiting this localized technique to assess in-situ measurements of the FFC activity. Instead of observing the corrosion behavior of defective coatings, as it is commonly done for instance in the field of self-healing protective coatings, [41,46], this work wanted to exploit a similar procedure to derive information about what is going on underneath the paint assuming partially negligible the effect of the organic layer damage. In this manner, new insights into the corrosion mechanism at the stack were reported. Several papers investigate FFC using SKP, while in this work, we propose the use of SVET for the first time. Moreover, to the best of our knowledge, it is the first time that SECM has been used in situ inside a FFC filament to investigate the local environment. The discussed findings are of crucial importance in the design of a suitable mitigation strategy for any coating system in atmospheric corrosion.

Furthermore, with the aim to validate the outcomes of the SVET analysis, local micropotentiometric pH measurement was performed, taking advantage of the potentiometric response of an antimony microelectrode positioned inside the coating artificial defects in an experimental setup similar to the SVET. Thanks to the variation of the potential of this material sensitive to the decreasing tendency to form Sb_2O_3 on its surface in more acidic environments, measurements of the pH in the anolyte and catholyte inside the filaments were performed [29,37,50–53].

Aiming to collect some in-situ measurements of the electrochemical activity ruling FFC on organic coated steel, we determined in this work the precise location of the anodic and cathodic areas and we determined the pH values developed at the metal-paint interface along the filament. Furthermore, the nature of the current flow turned out to be reliably assessed and correlated well with the pH measurements. Thereby the FFC mechanism has been depicted more comprehensively, trying to bridge the gap in the current literature and helping to validate some hypotheses made during the last decades of research. Besides the results presented relative to FFC, this study stands as a novel approach to exploit some already established techniques to investigate corrosion mechanisms of coated metals.

2. Materials and methods

2.1. Coated samples preparation

Mild steel substrates (Q-Panel R-36) were prepared by acid pickling (2 M HCl for 20 min) and coated with a commercial two-component polyamide-based clearcoat (supplied by Palini Vernici, Lovere BG, Italy) producing a dry layer of ca. 50 μm thickness after 1 h of curing at 60 °C. A scratch of 1 mm width and 60 mm length was introduced in the coating to the metal substrate with a scalpel, and the edges of the panels were sealed with tape to prevent cut-edge early damage. Consequently, the samples were placed in neutral salt spray chamber [54] for 5 h for chloride contamination, and aged at 40 °C and 80% relative humidity in compliance with ASTM 2803 standard [55] for 500 h obtaining filiform corrosion morphology steadily developed away from the artificial defect.

2.2. SVET measurements

The SVET instrument used was manufactured by Applicable Electronics (Forestdale, MA, USA). The adopted probe was a Pt/Ir (80%/20%) wire platinized to produce a platinum-black deposit of 10–20 μm diameter. The current maps were collected on a selected area following the mechanical perforation of the coating in precise spots of interest in the sample. The data were collected both on single-holed specimens and multiple defects to be aware of the possible effect of galvanic coupling on the entity of the signals and their magnitude. The probe vibration was set in a plane perpendicular to the sample with an amplitude of 40 μm in both Y and Z directions. A video camera connected to an optical microscope was utilized to set a controlled distance between the sample and the probe distance and to select the area of interest for mapping. The probe was set at 150 μm height from the sampled area by the following procedure using the optical microscope built into the system that is provided with a video camera. After focusing the camera on the sample surface, the focal point was moved up by the selected distance of 150 μm through a motorized system. Then the probe tip was moved to place it in focus matching the desired sample-probe distance. The electrochemical cell contained also two platinum wires for potential reference purposes. Over the coated specimen a plastic cylinder of 30 mm diameter is glued to contain the testing solution covering it with a height of electrolyte of approximately 5 mm. All the measurements were made in naturally aerated 10 mM NaCl solution at room temperature. Taking advantage of calibration procedures [42] the measured potentials were converted into current density values knowing the conductivity of the testing electrolyte (748 Ω cm). The ionic current maps were constituted by 961 points from a 31 × 31 measurement matrix along X and Y axis that was scanned following a meandering path from left to right and top to bottom. The sensed area dimensions varied depending on the shape of the corrosion analyzed and the detail considered, however, the time needed to complete the single measurement was always comprised between 3 and 5 min. The measurements were performed on several defected points (100–200 μm diameter) produced through the coating layer in some precise spots of interest in the sample. The coating holes were created by a nail just before the tip positioning procedure and subsequent filling of the cell with the test electrolyte. Hence, the data collection started with an estimated delay of 1–3 min from perforation. Images of the mapped surface were captured before and after recording each SVET map.

2.3. Micropotentiometric pH measurements

The potentiometric pH response of an antimony microelectrode was exploited to evaluate the liquid environment developed at the coating-metal interface along the corroding filament. The electrodes consisted of an outer capillary made of borosilicate glass in which a wire of high-purity antimony (10 mm length and 0.1 mm in diameter). This wire was inserted in the conical end of the capillary tube and the two parts were sealed with Loctite adhesive based on polymethyl methacrylate (Henkel, Düsseldorf, Germany). The exposed active disk areas were measured to have a diameter of 0.1 mm after a polishing stage. Liquid mercury and a copper wire were placed inside the capillary to guarantee the electrical connection.

The measurements of the potentials were taken in two different electrolytes. The first employs an electrochemical cell similarly built as in the SVET measurements where the reference electrode, in this case, was an Ag/AgCl/3 M KCl immersed in a 10 mM NaCl solution and the working was the antimony tip itself. In the second set up the liquid electrolyte was substituted by a gel-like agar-agar saturated in KCl. The perforation of the filament cover was performed through the jellified layer already covering the sample to limit the eventual disruption of the system due to exposure to the atmosphere and to the liquid electrolyte stages occurring in the other case. In both configurations, the sensing electrode was carefully placed as close as possible to the previously introduced coating defect, exploiting the motorized positioning system and a video camera, in order to be in contact with the metal paint liquid environment. Any movement of the sensing probe during the data collection in the case of a liquid environment was made possible by a step movement set in the motorized apparatus. In this experiment, one single spot was evaluated for each sample to prevent mixing effects from altering the local pH through the sensing environment. The values of pH were derived from the potential measurements at the antimony probe after a calibration procedure based on 6 points from 11.5 to 3 using certified buffer solutions as reference standards.

3. Results and discussion

3.1. SVET analysis on a perforated coating along the filiform filament

The SVET analysis is able to detect the ionic currents flowing in an electrolyte by detecting the electric fields generated by ions moving in the test solution. The vibrating probe is sensitive to the concentration gradients of ions caused by the evolution of corrosion. The outcome is zero in the bulk solution far from the sample or over an intact organic coated sample, but where a defect is present in the protective layer, ion flow can arise from the corrosion process. Furthermore considering the direction of the ionic currents it is possible to distinguish between the different electrochemical reactions involved and spatially resolve the anodic and cathodic active regions [23,33,35,36,45]. Typically, anodic sites in corroding metals are characterized by metal oxidation and the consequent release of cations resulting in a positive ionic current coming out of the surface. On the other hand, the coupled cathodes host the reduction reaction, usually the oxygen reduction in an aerated neutral environment, by triggering the consumption of dissolved O_2 in the electrolyte solution, leading to the generation of hydroxyl ions, and a related negative ionic current.

Fig. 1 shows an SVET map of a sample with three artificial defects simultaneously made through the coating, two of them at locations in the filament head, and one on the still intact coating. The scan started ca. 3 min after the perforation stage and approximately after 1 min immersion in the naturally aerated test solution. With this approach, some differences in electrochemical activity in particular regions of the filament could be distinguished. Positive and negative ionic currents were measured in the green-colored head and the brownish tail, respectively. Additionally, the surface surrounding the exposed metal in the scratch and the filament did not contribute any electric field, evidence that the pristine organic layer was protective and acted as an insulator. These signals can be assigned to the related anodic (positive) and cathodic (negative) corrosion reactions still evolving under the coating despite the time passed between the creation of the defects creation and the actual scan measurement. The oxidation reaction (Eq. 1) produces Fe(II) cations that flow from the defect towards the bulk electrolyte thanks to the concentration gradient. On the other hand, the reduction of oxygen, which is assumed to be the main cathodic event in these aerated neutral conditions, releases the negatively charged hydroxyl ions, which diffuse into the test solution and cause a charge movement of the opposite sign (Eq. 2).

$$Fe \rightarrow Fe^{2+} + 2e^{-} \quad (1)$$

$$O_2 + 2\,H_2O + 4e^{-} \rightarrow 4OH^{-} \quad (2)$$

Moreover, the perforated spot placed in the pristine coated sample surface in front of the advancing head of the filament under study (which is surrounded by a green square in Fig. 1b) showed a slightly cathodic character. However, this signal was much less intense, and it could be attributed not to an actual cathodic zone related to the growing FFC, but more likely to the freely corroding metal directly exposed to the aggressive solution being electrochemically activated as a result of exposure to the test electrolyte. We are led to believe the sign of the signal in this spot is randomly determined by the evolution of a general

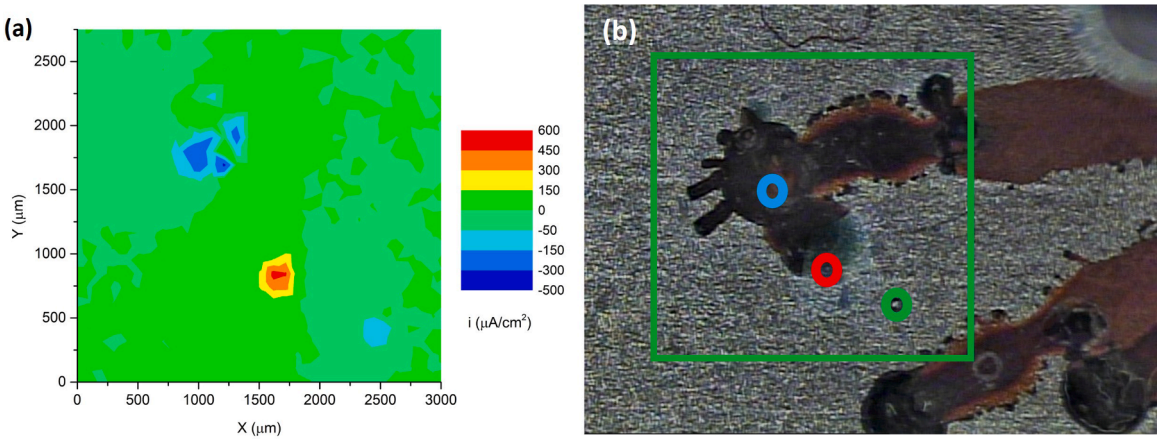

Fig. 1. Ionic current map in μA/cm2 obtained from SVET after 1 min immersion in 10 mM NaCl air-saturated aqueous electrolyte (a), and optical micrograph of the mapped square area with three perforated circular defects located in the brown-colored tail, green-colored leading head, and pristine uncorroded surface (b). Tip-substrate distance: 150 μm.

corrosion process as an early stage of cathodic delamination since further measurements on other samples damaged in similar regions presented an anodic response (Supplementary data S1). In all these cases, the magnitude of the current density was always far smaller than the peaks at the corroded areas in the filaments. The reproducibility of the opposite current density signals coming from the areas attributed to anodic and cathodic activity turns out to be reliable on the several replicant measurements on different samples and filaments. As proof of concept, an additional map obtained in similar conditions as Fig. 1 is provided in Supplementary data S1.

As reported by similar studies, when a coated metal with multiple defects in the protective layer is immersed in the conductive testing solution, a galvanic coupling between the holidays can develop [34,56,57]. The possibility of having this undesired contribution was present in the chosen setup, therefore tests were also made when the scans were collected on a single defect in each sample in order to avoid any galvanic

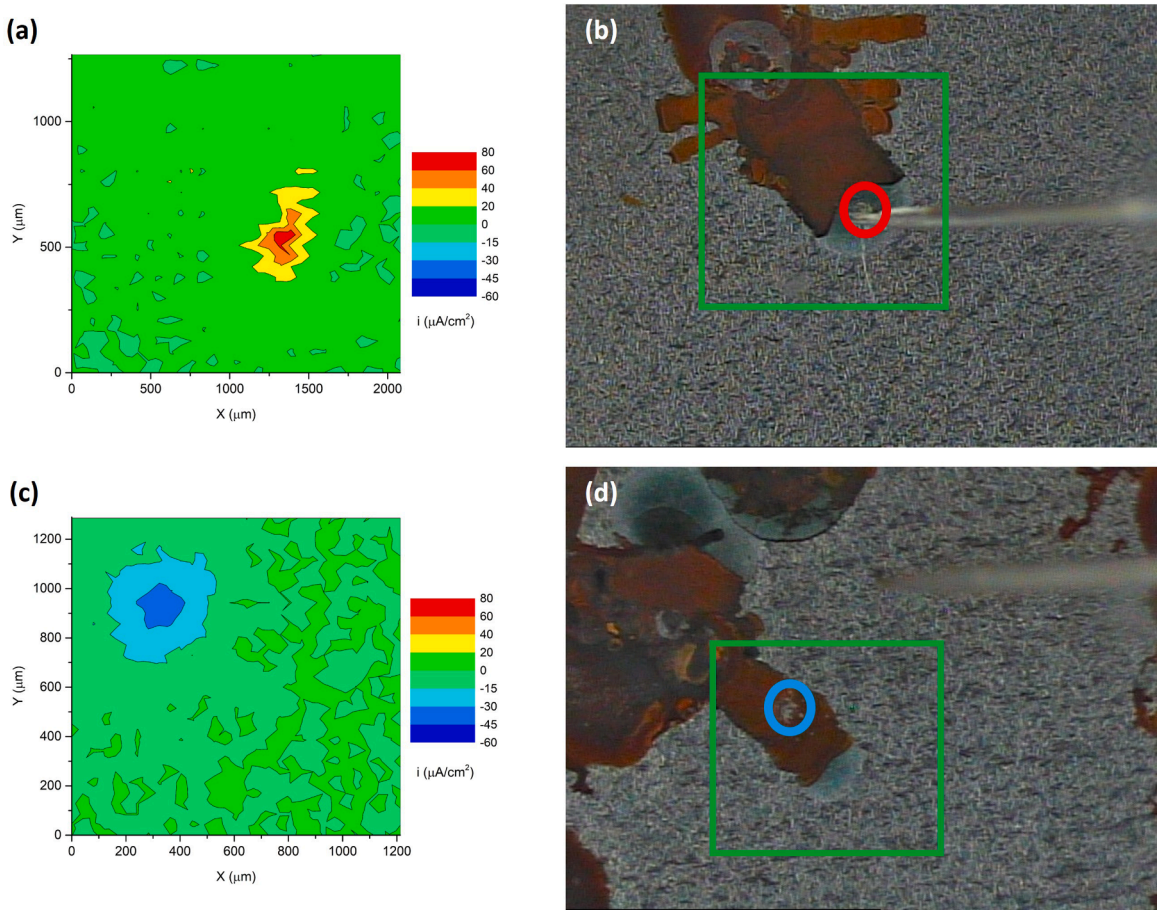

Fig. 2. Ionic current maps in μA/cm^2 obtained from SVET after 1 min of immersion in 10 mM NaCl air-saturated aqueous electrolyte (a) and (c). On the right, the related optical micrographs of the mapped square area are reported together with the single circular artificial defect in the green-colored leading head (b) and in the brown-colored tail (d). Tip-substrate distance: 150 μm.

coupling between multiple active metallic sites. As shown by the SVET maps in Fig. 2, the outcomes based on the sign of the current as an indication of the dominant redox half-reaction in each spot seem to confirm the observations raised in the case of the multiple hole arrangement of Fig. 1. That is, the results confirmed that the head behaves as an anode (Fig. 2a) and the tail as a cathode (Fig. 2b). Furthermore, the outcomes seem not to be significatively affected, at least from a qualitative point of view by the choice of single or multiple holes in a given filament. However, this study proves to be non-quantitative as different filaments return different orders of magnitude of ionic current, probably due to differences in filament activity, the morphology of the artificial holes, and distances of the tip from the surface caused by corrosion bulging. Therefore, at this stage, it was not reliable to precisely estimate the potential difference between anode and cathode or to obtain hints about the magnitude of the driving force in terms of corrosion current, but it is a still powerful procedure for mapping the reactions operating along the filament.

The leading head is characterized by a distinctive green color given by the corrosion product oxidation state at the interface. This complex mixture of oxides and hydroxides is known as "green rust" [58–60]. Its formation is characterized by a gradient along the propagating direction (Fig. 3b). The rear part of the head, confined by the typical "V-shape" border with the brownish tail, appears darker due to the more abundant presence of oxidation products. At the same time, the more transparent front represents the outpost of the anodic undermining where the loss of coating adhesion occurs. This is translated into ionic current density in Fig. 3a where two defects in the head testify that the color gradient also represents a variation in the magnitude of the anodic activity. The anodic nature of the leading part of the filament was confirmed, and the most reactive portion of the element occurred at the back zone of the head.

It should be noted that the most interesting measurements in terms of FFC characterization were the first made after solution immersion. Over time, the signals recorded from the different holes tend to equalize and the system deviates more and more from the natural situation with the intact coating covering the filament. Furthermore, the increasing deposits of rust could shield the ionic movement and stagger the outcomes [43]. Indeed, monitoring the evolution in immersion time, the gradient between the two areas of the head progressively disappeared and the activity was equalized since no more oxygen gradient would be present along the filament and the FFC mechanism could not be sustained anymore after 1 h of immersion (Supplementary data S2). From the observation of the temporal evolution of the system, it was possible to obtain some hints on the time frame available for the application of the approach presented in this work.

According to an SKP study by Leblanc and Frankel [10], the tail has a constant Volta potential in agreement with the SVET analysis in Fig. 4, which can be identified as cathodic activity. The different current density magnitudes along the tail are assumed to be experimental artifacts derived from the poorly reproducible perforation stage.

In our previous publication [2], an electrochemical simulation study based on zero-resistance amperometry was reported showing the dependence of corrosion current on the cathode-anode area ratio. At that point, two hypotheses were proposed by examining the results. Since the rate of filament propagation was found to be constant and the greenish zone of the head was observed to be stable over time, the growing tail had to behave as an inactive deposit of corrosion products, and either both electrochemical half-cell reactions were hosted in the moving head, or the tail had to host the cathodic reactions homogenously while decreasing the corrosion current density distributed along it over time. This last proposal seems to coincide with all the findings of this work.

3.2. *pH evaluation at anodic and cathodic sites using the antimony microelectrode*

The calibration of the antimony electrode was based on measuring the potential in six different buffer solutions. The procedure sequence has followed an increased acidity starting from pH 11.5–3. The obtained plot is given in Supplementary Data S3, in which the measured potential varies linearly with the pH of the solution. The slope of the line was 49.6 mV/pH unit. This value was in agreement with the reports available in the literature, which give a range of 40–50 mV/pH unit for polycrystalline antimony [50,52].

The antimony electrode was used as a pH sensor by placing it close to the artificial defect made in each tested sample while immersed in 10 mM NaCl solution during the measurements. The microelectrode was first moved in the Z-direction to approach the coating surface from an initial distance of 5 mm. Data were collected during its trajectory for 2000 s to assess any eventual drifts in stabilization over time and to highlight the different environments found by the probe when traveling from the bulk electrolyte to the corroding interface. Once the measured value reached a stationary condition, the tip was returned to the initial position and repositioned following the same trajectory but moving in the opposite direction. By approaching the environment created at the interface by the corrosion products deposits, hints about the electrochemical activity could be derived. Fig. 5 shows the outcomes of this procedure for three different cases: tail, head, and the steady bulk testing solution (blank). The pH of the test solution far away from the sample was confirmed to agree well with the value measured using a

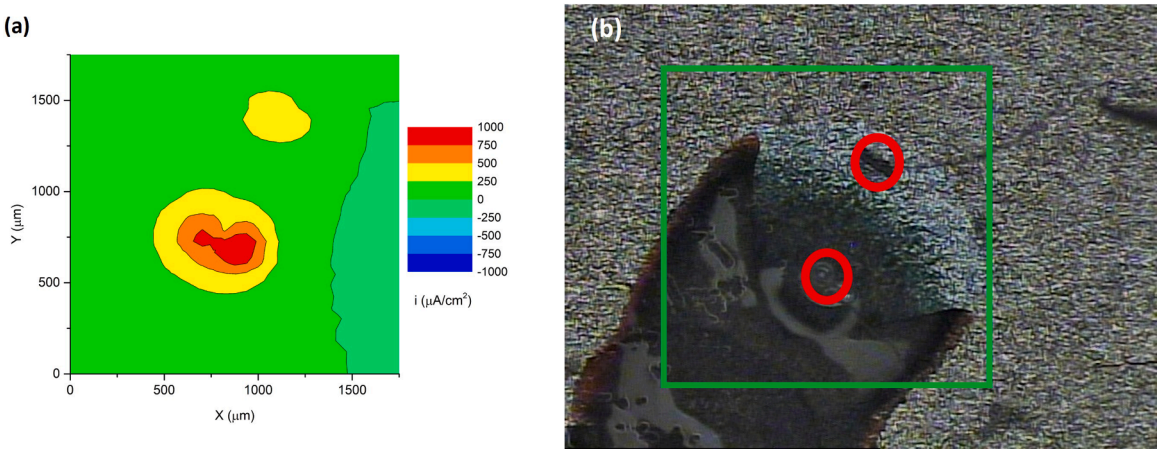

Fig. 3. Ionic current map in μA/cm^2 obtained from SVET after 1 min immersion in 10 mM NaCl air-saturated aqueous electrolyte (a), and optical micrograph of the mapped square area with two circular artificial defects in the green-colored leading head, in the lighter anterior halo and the darker rear position respectively (b). Tip-substrate distance: 150 μm.

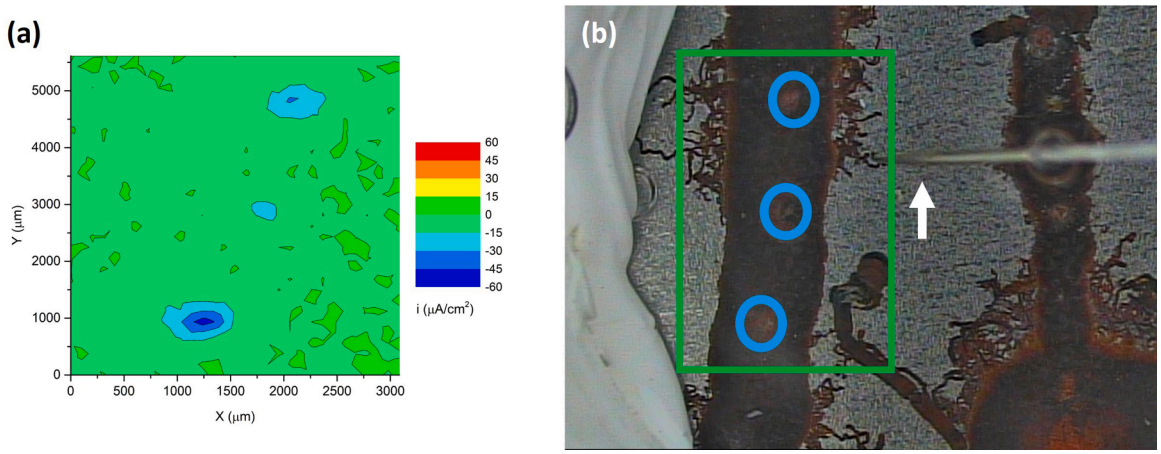

Fig. 4. Ionic current map in μA/cm^2 obtained from SVET after 1 min immersion in 10 mM NaCl air-saturated aqueous electrolyte (a), and optical micrograph of the mapped square area with three circular artificial defects along the corroded filament tail (b). The propagating direction is indicated by the white arrow. Tip-substrate distance: 150 μm.

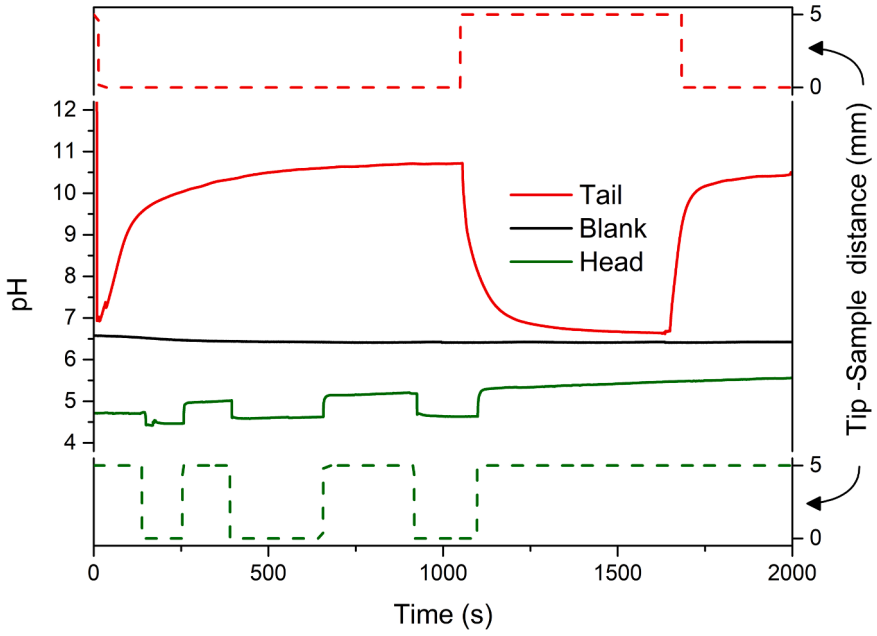

Fig. 5. Local potentiometric measurement of pH vs. immersion time for the antimony electrode moving over a hole perforated on the filament head (solid line in green), over a hole perforated in the filament tail (solid line in red), and in the bulk of the 10 mM NaCl test solution (blank condition, solid line in black). The dashed lines both at the bottom (in green) and top (in red) of the graph represent the alternating approach and retrieval trajectories made by the sensing tip in the Z-direction relative to the sample surface (taken as 0 mm) that the antimony electrode traveled when placed just above the perforated holes in the head and the tail of the filament, respectively.

conventional pH-meter provided with a glass electrode (namely, 6.5). The measurement of the pH value in the proximity of the hole perforated in the tail of the filament took more time to stabilize than the acidic value measured in the hole produced in the head. The obtained values of 11.5 and 4.5, respectively, support the SVET outcomes since the production of hydroxyl ions was detected in the tail due to the cathodic reaction of oxygen redaction. The measured values are in agreement with the literature data on pH estimation obtained by simply removing the paint [3,9,15,61] and the data showed good reproducibility. A supplementary replicate of all three measurements discussed is provided in Supplementary Data S4. At the leading part of the head, the acidic pH confirms both the presence of an oxygen-depleted environment and the occurrence of a hydrolysis reaction to produce Fe^{3+} cations, which is given by Eq. (3) [62].

$$Fe(H_2O)_6^{3+}\,(aq) \rightarrow Fe(H_2O)_5\,(OH)^{2+}\,(aq) + H^{+}\,(aq) \quad (3)$$

The described findings further support the location of active sites observed by SVET and provide a novel investigation method for testing interfacial pH in the case of organic-coated metals.

Since the scanning micropotentiometric analysis was performed in a liquid environment, the main concern with this procedure was the possible dilution effect due to exposure of the local environment and corrosion products below the perforated cover after the coating perforation stage to the largest volume of test electrolyte placed above the sample required for potentiometric measurement. In addition, partial oxidation of the species at the interface, especially the green rust rich in Fe^{2+} in the head [62], could occur after the perforation stage. Considering these experimental limitations, the experiment was repeated in a similar manner, replacing the saline test solution with a jellified electrolyte of agar-agar saturated in KCl. In this way, the mobility of the

species coming from the holes perforated in the organic layer should be decreased compared to the liquid medium, and the impact of dilution should be reduced. Next, the choice to make the holes in the coating with the gel already covering the surface of the coated sample likely reduced the exposure to atmospheric oxygen that could reach the damaged metal-paint interface, thus attenuating the variation in pH derived from such an oxidation process. In this configuration, no movement of the antimony microelectrode relative to the surface of the sample was made this time, and data were recorded by placing it close to the corresponding artificial defect and keeping its position fixed. In this configuration, the potential detected in the antimony tip was monitored over time until it stabilized. It should be noted that the pH values recorded after 6000 s coincided with those evaluated before using this method with the sample immersed in the liquid electrolyte (Fig. 6). That is, the pH amounted to 10.3 for the corrosion products in the tail, and 4.7 for the green rust in the head.

3.3. FFC model

The experimental outcomes of this work clarify and refine the model of FFC on organic coated steel. A comprehensive literature review of the models available in the literature and an updated schematic of the main factors at stake have been already included in a recent publication [2]. In the cited work the mechanism depicted was based on some hypotheses by other authors in the years and has not yet been experimentally verified. This study based on in-situ localized techniques wants to go beyond these experimental lacks. Fig. 7a is a further improved representation of FFC propagation. On the basis of the verified location of anodic and cathodic sites by SVET and pH measurements the model is updated attributing to the entire green-colored region confined within the V-shaped border (Fig. 7b). The gradient in color from the transparent leading delamination edge to the back portion of the head, where the green becomes more intense and darker, corresponds to a gradient in anodic activity assessed by the different intense current signals of Fig. 3. The coupled cathode lies along the tail, which is the main path for oxygen supply through the permeable brown colored corrosion products [2,62]. The consideration of the oxygen availability is in agreement also with the pH evaluation, since the cathodic reaction is supposed to produce a certain alkalinity and the tail thanks to the oxygen abundance meets all these findings. On the other hand, the oxygen depletion of the

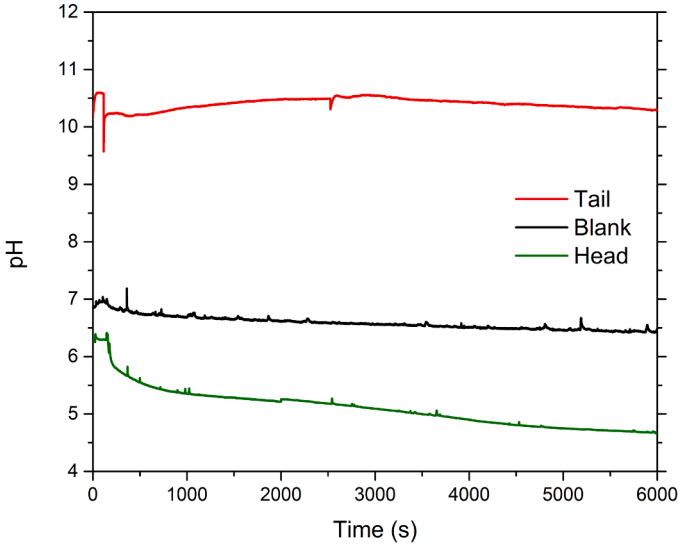

Fig. 6. Local potentiometric measurement of pH vs. immersion time with the antimony electrode placed close to the holes perforated in the head (in green), and tail (in red) of the filament, and pH recorded in the bulk agar-agar gel saturated in KCl used as test electrolyte (blank, in black).

head matches the anodic character attributed to this site. The differential aeration is accepted to be the main driving force of the FFC propagation, it causes spatial separation of electrochemical environments along the filament [1,3]. This fact triggers the creation of spatially distinct anodic and cathodic reactions. Due to the reactions the delaminated metal-paint interface is characterized by diverse pH levels, from acidic (anode) to alkaline (cathode). All these features, experimentally assessed in this work, accomplish the definition of the mechanism. From a corrosion prevention point of view, the mitigation strategies have to be tailored taking into account the anodic nature of the leading delamination front, and the acidic environment developed.

4. Conclusions

To our knowledge, the scanning vibrating electrode technique and scanning micropotentiometry using an antimony microelectrode were employed for the first time in the study of the filiform corrosion occurring on organic-coated steel. A novel experimental methodology was developed to investigate the distribution of electrochemically active sites in the filaments, and the location of the anodic and cathodic reactions building up the FFC process was spatially resolved for the first time. The entire green head confined in the so-called “V-shape” border with the brown corrosion products was shown to be anodic, and the intensity of the activity seemed to be higher in the darker back part compared to the leading halo. The delamination front was confirmed to be of an anodic character, disproving some models available in the literature where a cathodic delamination outpost is theorized. The role of the tail in the propagation process was not clear to date, but in this work the entire length of the brown filament tail was found to be electrochemically active towards the reduction of oxygen (acting as the cathodic site), thus supporting filament propagation.

The SVET maps presented here are still regarded to be mostly of a qualitative character since the magnitude of the current values was found to be greatly influenced by a combination of different filament sizes and morphologies. Furthermore, the experimental procedure employed here is still to be optimized to accurately control the direction and strength employed to perforate the coating cover in the filaments, in order to reduce some uncontrolled variability in size and morphology that prevented a more quantitative comparison of the outcomes at this stage.

By means of a spatially-resolved potentiometric measurement using an antimony microelectrode, the pH values developed along the different reaction sites in the filament were determined in situ. The pH values were found to be 4.5 (acidic) in the head, and 10.5 (alkaline) in the tail. The distinct pH values found here corroborate the location of anodic and cathodic sites revealed by SVET maps. Anodic activities generated an acidic environment in the filament head at the metal-paint interface, while the cathodic reduction of oxygen was responsible for the alkalinization of the tail.

The new methodology based on coupling SVET and scanning micropotentiometry was found to be adequate for investigating the corrosion mechanism of filiform corrosion processes developing on organic coated metals, and it can be implemented to study many other case studies where the presence of the polymeric layer shelters the phenomena occurring at the buried coating/substrate interface.

CRediT authorship contribution statement

Andrea Cristoforetti: Methodology, Investigation, Writing – original draft. **Michele Fedel:** Methodology, Writing – review & editing. **Stefano Rossi:** Methodology, Funding acquisition, Writing – review & editing. **Flavio Deflorian:** Resources, Funding acquisition. **Ricardo M. Souto:** Supervision, Funding acquisition, Methodology, Writing – review & editing. **Javier Izquierdo:** Methodology, Investigation, Writing – review & editing.

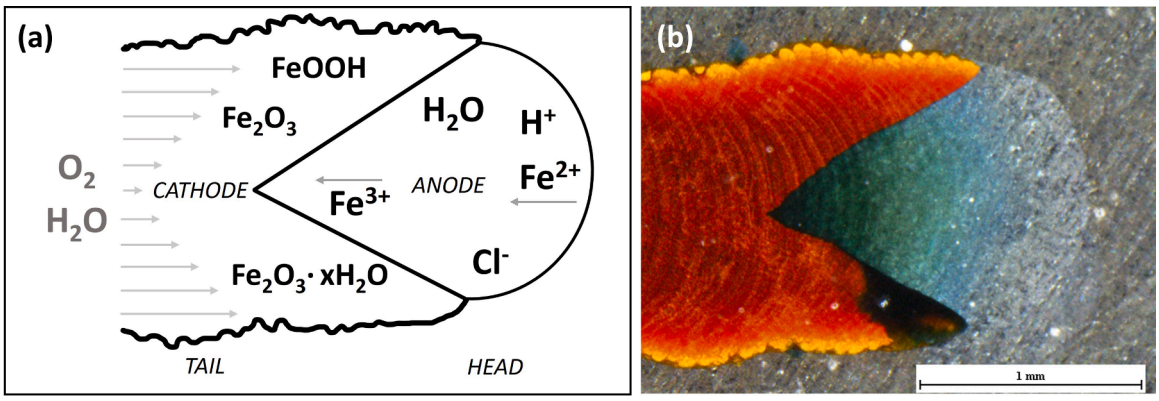

Fig. 7. Schematic representation of FFC mechanism (a) coupled with an example of filament appearance captured by optical imaging through the clearcoat (b).

Declaration of Competing Interest

The authors declare that they have no known competing financial interests or personal relationships that could have appeared to influence the work reported in this paper.

Data Availability

Data will be made available on request.

Acknowledgments

R.M.S. and J.I. acknowledge funding by the Spanish Ministry of Science and Innovation (MICINN, Madrid, Spain), and the European Regional Development Fund (Brussels, Belgium) MCIN/AEI/10.13039/501100011033/FEDER, UE under grant PID2021-127445NB-I00.

Appendix A. Supporting information

Supplementary data associated with this article can be found in the online version at doi:10.1016/j.corsci.2023.111669.

References

[1] G. Williams, H. N. McMurray, D. Hayman, P. C. Morgan, Time-lapse potentiometric imaging of active filiform corrosion using a scanning Kelvin probe technique, PhysChemComm 4 (2001) 1–6, https://doi.org/10.1039/b100835h.
[2] A. Cristoforetti, S. Rossi, F. Deflorian, M. Fedel, An electrochemical study on the mechanism of filiform corrosion on acrylic-coated carbon steel, Prog. Org. Coat. 179 (2023), 107525, https://doi.org/10.1016/j.porgcoat.2023.107525.
[3] A. Bautista, Filiform corrosion in polymer-coated metals, Prog. Org. Coat. 28 (1996) 49–58, https://doi.org/10.1016/0300-9440(95)00555-2.
[4] G. Williams, H.N. McMurray, The mechanism of group (I) chloride initiated filiform corrosion on iron, Electrochem. Commun. 5 (2003) 871–877, https://doi.org/10.1016/J.ELECOM.2003.08.008.
[5] S.B. Lyon, R. Bingham, D.J. Mills, Advances in corrosion protection by organic coatings: what we know and what we would like to know, Prog. Org. Coat. 102 (2017) 2–7, https://doi.org/10.1016/j.porgcoat.2016.04.030.
[6] A. Cristoforetti, S. Rossi, F. Deflorian, M. Fedel, Comparative study between natural and artificial weathering of acrylic-coated steel, aluminum, and galvanized steel, Mater. Corros. (2023) 1–10, https://doi.org/10.1002/maco.202313858.
[7] W. Funke, Blistering of paint films and filiform corrosion, Prog. Org. Coat. 9 (1981) 29–46, https://doi.org/10.1016/0033-0655(81)80014-3.
[8] R.T. Ruggeri, T.R. Beck, An analysis of mass transfer in filiform corrosion, Corrosion 39 (1983) 452–465, https://doi.org/10.5006/1.3581907.
[9] W.H. Slabaugh, M. Grotheer, Mechanism of filiform corrosion, Ind. Eng. Chem. 46 (1954) 1014–1016, https://doi.org/10.1021/ie50533a053.
[10] P.P. Leblanc, G.S. Frankel, Investigation of filiform corrosion of epoxy-coated 1045 carbon steel by scanning kelvin probe force microscopy, J. Electrochem. Soc. 151 (2004) B105–B113, https://doi.org/10.1149/1.1641038.
[11] R. Catubig, M. Seter, W. Neil, M. Forsyth, B. Hinton, Effects of corrosion inhibiting pigment lanthanum 4-hydroxy cinnamate on the filiform corrosion of coated steel, J. Electrochem. Soc. 158 (2011) C353–C358, https://doi.org/10.1149/2.012111jes.
[12] E.L. Koehler, Influence of contaminants on the failure of protective organic coatings on steel, Corrosion 33 (1977) 209–217, https://doi.org/DOI:10.5006/0010-9312-33.6.209.
[13] J.M.C. Mol, B.R.W. Hinton, D.H. Van Der Weijde, J.H.W. De Wit, S. Van Der Zwaag, A filiform corrosion and potentiodynamic polarisation study of some aluminium alloys, J. Mater. Sci. 35 (2000) 1629–1639, https://doi.org/10.1023/A:1004795528090.
[14] J.H.W. de Wit, New knowledge on localized corrosion obtained from local measuring techniques, Electrochim. Acta 46 (2001) 3641–3650, https://doi.org/10.1016/S0013-4686(01)00642-9.
[15] W.H. Slabaugh, W. Dejager, S.E. Hoover, L.L. Hutchinson, Filiform corrosion of aluminum, J. Paint Technol. 44 (1972) 76–83.
[16] G. Bierwagen, D. Tallman, J. Li, L. He, C. Jeffcoate, EIS studies of coated metals in accelerated exposure, Prog. Org. Coat. 46 (2003) 149–158, https://doi.org/10.1016/S0300-9440(02)00222-9.
[17] I.C.P. Margarit-Mattos, EIS and organic coatings performance: revisiting some key points, Electrochim. Acta 354 (2020), 136725, https://doi.org/10.1016/j.electacta.2020.136725.
[18] A. Amirudin, D. Thieny, Application of electrochemical impedance spectroscopy to study the degradation of polymer-coated metals, Prog. Org. Coat. 26 (1995) 1–28, https://doi.org/10.1016/0300-9440(95)00581-1.
[19] G. Grundmeier, W. Schmidt, M. Stratmann, Corrosion protection by organic coatings: electrochemical mechanism and novel methods of investigation, Electrochim. Acta 45 (2000) 2515–2533, https://doi.org/10.1016/S0013-4686(00)00348-0.
[20] A. Alizadeh Razin, B. Ramezanzadeh, H. Yari, Detecting and estimating the extent of automotive coating delamination and damage indexes after stone chipping using electrochemical impedance spectroscopy, Prog. Org. Coat. 92 (2016) 95–109, https://doi.org/10.1016/J.PORGCOAT.2015.11.023.
[21] A.S. Castela, A.M. Simões, Assessment of water uptake in coil coatings by capacitance measurements, Prog. Org. Coat. 46 (2003) 55–61, https://doi.org/10.1016/S0300-9440(02)00190-X.
[22] A. Miszczyk, K. Darowicki, Water uptake in protective organic coatings and its reflection in measured coating impedance, Prog. Org. Coat. 124 (2018) 296–302, https://doi.org/10.1016/J.PORGCOAT.2018.03.002.
[23] A. Cristoforetti, S. Rossi, F. Deflorian, M. Fedel, On the limits of the EIS low-frequency impedance modulus as a tool to describe the protection properties of organic coatings exposed to accelerated aging tests, Coatings 13 (2023), https://doi.org/10.3390/coatings13030598.
[24] J.J. Santana, J. González-Guzmán, J. Izquierdo, S. González, R.M. Souto, Sensing electrochemical activity in polymer-coated metals during the early stages of coating degradation by means of the scanning vibrating electrode technique, Corros. Sci. 52 (2010) 3924–3931, https://doi.org/10.1016/j.corsci.2010.08.010.
[25] N. Khayatan, M. Rohwerder, A new insight into the rate determining step of cathodic delamination, Corros. Sci. 202 (2022), 110311, https://doi.org/10.1016/j.corsci.2022.110311.
[26] A.P. Nazarov, D. Thierry, Scanning kelvin probe study of metal/polymer interfaces, Electrochim. Acta 49 (2004) 2955–2964, https://doi.org/10.1016/J.ELECTACTA.2004.01.054.
[27] W. Schmidt, M. Stratmann, Scanning Kelvinprobe investigations of filiform corrosion on aluminium alloy 2024-T3, Corros. Sci. 40 (1998) 1441–1443, https://doi.org/10.1016/S0010-938X(98)00044-4.
[28] V. Upadhyay, D. Battocchi, Localized electrochemical characterization of organic coatings: a brief review, Prog. Org. Coat. 99 (2016) 365–377, https://doi.org/10.1016/j.porgcoat.2016.06.012.
[29] J.J. Santana, J. Izquierdo, R.M. Souto, Uses of scanning electrochemical microscopy (SECM) for the characterization with spatial and chemical resolution of thin surface layers and coating systems applied on metals: a review, Coatings 2022 (12) (2022) 637, https://doi.org/10.3390/coatings12050637.
[30] N. Jadhav, V.J. Gelling, The use of localized electrochemical techniques for corrosion studies, J. Electrochem. Soc. 166 (2019) C3461–C3476, https://doi.org/10.1149/2.0541911jes.

[31] N.A. Payne, L.I. Stephens, J. Mauzeroll, The application of scanning electrochemical microscopy to corrosion research, Corrosion 73 (2017) 759–780, https://doi.org/10.5006/2354.
[32] R. Oltra, V. Maurice, R. Akid, P. Marcus, Local probe techniques for corrosion. Research, Elsevier, 2014.
[33] R.S. Lillard, Analytical Methods in Corrosion Science and Engineering, CRC, Boca Raton, 2006, pp. 571–604.
[34] A.C. Bastos, O.V. Karavai, M.L. Zheludkevich, K.A. Yasakau, M.G.S. Ferreira, Localised measurements of pH and dissolved oxygen as complements to SVET in the investigation of corrosion at defects in coated aluminum alloy, Electroanalysis 22 (2010) 2009–2016, https://doi.org/10.1002/elan.201000076.
[35] A.C. Bastos, M.G. Ferreira, A.M. Simões, Corrosion inhibition by chromate and phosphate extracts for iron substrates studied by EIS and SVET, Corros. Sci. 48 (2006) 1500–1512, https://doi.org/10.1016/j.corsci.2005.05.021.
[36] S. Sheikholeslami, G. Williams, H.N. McMurray, L. Gommans, S. Morrison, S. Ngo, D.E. Williams, W. Gao, Cut-edge corrosion behavior assessment of newly developed environmental-friendly coating systems using the Scanning Vibrating Electrode Technique (SVET), Corros. Sci. 192 (2021), 109813, https://doi.org/10.1016/j.corsci.2021.109813.
[37] J. Izquierdo, L. Nagy, S. González, J.J. Santana, G. Nagy, R.M. Souto, Resolution of the apparent experimental discrepancies observed between SVET and SECM for the characterization of galvanic corrosion reactions, Electrochem. Commun. 27 (2013) 50–53, https://doi.org/10.1016/j.elecom.2012.11.002.
[38] F. Mahdavi, M. Forsyth, M.Y.J. Tan, Techniques for testing and monitoring the cathodic disbondment of organic coatings: an overview of major obstacles and innovations, Prog. Org. Coat. 105 (2017) 163–175, https://doi.org/10.1016/J.PORGCOAT.2016.11.034.
[39] J.B. Jorcin, E. Aragon, C. Merlatti, N. Pébère, Delaminated areas beneath organic coating: a local electrochemical impedance approach, Corros. Sci. 48 (2006) 1779–1790, https://doi.org/10.1016/J.CORSCI.2005.05.031.
[40] R.S. Lillard, J. Kruger, W.S. Tait, P.J. Moran, Using local electrochemical impedance spectroscopy to examine coating failure, Corrosion 51 (1995) 251–259.
[41] A. Bastos, Application of SVET/SIET techniques to study healing processes in coated metal substrates, in: L. Klein, M. Aparicio, A. Jitianu (Eds.), Handbook of Sol-Gel Science and Technology: Processing, Characterization and Applications, Springer International Publishing, Cham, 2018, pp. 1727–1782, https://doi.org/10.1007/978-3-319-32101-1_138.
[42] G. Zhang, E. Jiang, L. Wu, A. Tang, A. Atrens, F. Pan, Active corrosion protection of phosphate loaded PEO/LDHs composite coatings: SIET study, J. Magnes. Alloy. 10 (2022) 1351–1357, https://doi.org/10.1016/j.jma.2021.03.008.
[43] R.M. Souto, Y. González-García, A.C. Bastos, A.M. Simões, Investigating corrosion processes in the micrometric range: a SVET study of the galvanic corrosion of zinc coupled with iron, Corros. Sci. 49 (2007) 4568–4580, https://doi.org/10.1016/j.corsci.2007.04.016.
[44] D.A. Worsley, H.N. McMurray, A. Belghazi, Determination of localised corrosion mechanisms using a scanning vibrating reference electrode technique, Chem. Commun. (1997) 2369–2370.
[45] T.E. Schmitzhaus, M.R.O. Vega, R. Schroeder, I.L. Muller, S. Mattedi, M. Taryba, J. C.S. Fernandes, C. de F. Malfatti, Localized corrosion behavior studies by SVET of 1010 steel in different concentrations of sodium chloride containing [m-2HEA][Ol] ionic liquid as corrosion inhibitor, Electrochim. Acta 419 (2022), 140385, https://doi.org/10.1016/j.electacta.2022.140385.
[46] A.C. Bastos, M.C. Quevedo, O.V. Karavai, M.G.S. Ferreira, Review—on the application of the scanning vibrating electrode technique (SVET) to corrosion research, J. Electrochem. Soc. 164 (2017) C973–C990, https://doi.org/10.1149/2.0431714jes.
[47] R. Souto, Y. González-Garcıa, S. González, G. Burstein, Damage to paint coatings caused by electrolyte immersion as observed in situ by scanning electrochemical microscopy, Corros. Sci. 46 (2004) 2621–2628, https://doi.org/10.1016/j.corsci.2004.06.00.
[48] J.J. Santana, M. Pähler, R.M. Souto, W. Schuhmann, Direct evidence of early blister formation in polymer-coated metals from exposure to chloride-containing electrolytes by alternating-current scanning electrochemical microscopy, Electrochim. Acta 77 (2012) 60–64.
[49] Y. Elkebir, S. Mallarino, D. Trinh, S. Touzain, Effect of physical ageing onto the water uptake in epoxy coatings, Electrochim. Acta 337 (2020), 135766.
[50] J. Izquierdo, L. Nagy, Á. Varga, J.J. Santana, G. Nagy, R.M. Souto, Spatially resolved measurement of electrochemical activity and pH distributions in corrosion processes by scanning electrochemical microscopy using antimony microelectrode tips, Electrochim. Acta 56 (2011) 8846–8850, https://doi.org/10.1016/j.electacta.2011.07.076.
[51] M. Al-Jeda, E. Mena-Morcillo, A. Chen, Micro-sized pH sensors based on scanning electrochemical probe microscopy, Micromachines 13 (2022) 2143, https://doi.org/10.3390/mi13122143.
[52] G. Nagy, L. Nagy, Electrochemical sensors developed for gathering microscale chemical information, Anal. Lett. 40 (2007) 3–38, https://doi.org/10.1080/00032710600867226.
[53] T.R. Ball, The antimony electrode in pH measurements, Trans. Electrochem. Soc. 72 (1937) 139–152, https://doi.org/10.1149/1.3493930.
[54] ASTM B117–19, Standard Practice for Operating Salt Spray (Fog) Apparatus, (2019). https://doi.org/10.1520/B0117–19.
[55] ASTM D2803–09, Standard Guide for Testing Filiform Corrosion Resistance of Organic Coatings on Metal, (2020). https://doi.org/10.1520/D2803–09R20.
[56] R.M. Souto, Y. González-García, S. González, In situ monitoring of electroactive species by using the scanning electrochemical microscope. Application to the investigation of degradation processes at defective coated metals, Corros. Sci. 47 (2005) 3312–3323, https://doi.org/10.1016/j.corsci.2005.07.005.
[57] R.M. Souto, J. Izquierdo, J.J. Santana, S. González, Scanning microelectrochemical techniques a highly sensitive route to evaluate degradation reactions and protection methods with chemical selectivity, Eur. J. Sci. Theol. (2013).
[58] J.M.R. Génin, P.H. Refait, M. Abdelmoula, Green rusts and their relationship to iron corrosion; a key role in microbially influenced corrosion, Hyperfine Interact. 139–140 (2002) 119–131, https://doi.org/10.1023/A:1021219021919.
[59] J.M.R. Génin, P. Refait, L. Simon, S.H. Drissi, Preparation and Eh-pH diagrams of Fe(II)-Fe(III) green rust compounds; hyperfine interaction characteristics and stoichiometry of hydroxy-chloride, -sulphate and -carbonate, Hyperfine Interact. 111 (1998) 313–318.
[60] M. Abdelmoula, P. Refait, S.H. Drissi, J.P. Mihe, J.M.R. Génin, Conversion electron Mössbauer spectroscopy and X-ray diffraction studies of the formation of carbonate-containing green rust one by corrosion of metallic iron in NaHCO3 and (NaHCO3 + NaCl) solutions, Corros. Sci. 38 (1996) 623–633, https://doi.org/10.1016/0010-938X(95)00153-B.
[61] G.M. Hoch, A review of filiform corrosion, Houston, TX, 1974.
[62] T.M. Watson, A.J. Coleman, G. Williams, H.N. McMurray, The effect of oxygen partial pressure on the filiform corrosion of organic coated iron, Corros. Sci. 89 (2014) 46–58, https://doi.org/10.1016/j.corsci.2014.08.004.